Calibrating a long-term meteoric ¹⁰Be delivery rate into eroding Western US glacial deposits by comparing meteoric and in situ-produced ¹⁰Be depth profiles

- 5 Travis Clow¹, Jane K. Willenbring^{1,2}, Mirjam Schaller³, Joel D. Blum⁴, Marcus Christl⁵, Peter W. Kubik⁵, Friedhelm von Blanckenburg²
 - ¹Department of Geological Sciences, Stanford University, Stanford, CA, USA
 - ²GFZ German Research Centre for Geosciences, Earth Surface Geochemistry, Telegrafenberg, 14473 Potsdam, Germany
- 10 ³Geodynamics, University of Tübingen, Wilhelmstraße 56, 72076 Tübingen, Germany
 - ⁴Department of Earth and Environmental Sciences, University of Michigan, Ann Arbor, MI, USA
 - ⁵ETH Zurich, Laboratory of Ion Beam Physics, HPK G23, Schafmattstrasse 20, ETH-Zurich, CH-8093 Zurich, Switzerland *Correspondence to*: Travis Clow (tclow@stanford.edu)

Abstract. Meteoric ¹⁰Be (¹⁰Be_{met}) concentrations in soil profiles have great potential as a geochronometer and a tracer of

Earth surface processes, particularly in fine-grained soils lacking quartz that would preclude the use of *in situ*-produced ¹⁰Be (¹⁰Be_{in situ}). One prerequisite for using this technique for accurately calculating rates and dates is constraining the delivery, or flux, of ¹⁰Be_{met} to a site. However, few studies to date have quantified long-term (i.e. millennial) delivery rates, and none have determined a delivery rate for an eroding soil. In this study, we compared existing concentrations of ¹⁰Be_{in situ} with new measurements of ¹⁰Be_{met} in eroding soils sampled from the same depth profiles to calibrate a long-term ¹⁰Be_{met} delivery rate.

We did so on the Pinedale (~21-25 ky) and Bull Lake (~140 ky) glacial moraines at Fremont Lake, Wyoming (USA) where age, grain sizes, weathering indices, and soil properties are known, as are erosion/denudation rates calculated from ¹⁰Be_{in situ}. After ensuring sufficient beryllium retention in each profile, solving for the delivery rate of ¹⁰Be_{met}, and normalizing for paleomagnetic and solar intensity variations over the Holocene, we calculate ¹⁰Be_{met} fluxes of 1.46 (± 0.20) x 10⁶ atoms cm⁻² y⁻¹ and 1.30 (± 0.48) x 10⁶ atoms cm⁻² y⁻¹ to the Pinedale and Bull Lake moraines, respectively, and compare these values to two widely-used ¹⁰Be_{met} delivery rate estimation methods that substantially differ for this site. Accurately estimating ¹⁰Be_{met} flux using these methods requires consideration of spatial scale as well as temporally varying parameters (i.e. paleomagnetic field intensity, solar modulation) to ensure the most realistic estimates of ¹⁰Be_{met}-derived erosion rates in future studies.

1 Introduction

¹⁰Be is a cosmogenic isotope with a half-life of 1.39 +/- 0.01 My (Chmeleff et al., 2010) and its meteoric form (¹⁰Be_{met}) is 30 produced in the atmosphere through spallation reactions as high-energy cosmic rays collide with target nuclei (i.e. ¹⁴N and ¹⁶O) in the atmosphere (Lal and Peters, 1967). ¹⁰Be_{met} is then delivered to Earth's surface via precipitation or as dry deposition at a flux of $0.1-2 \times 10^6$ atoms cm⁻² y⁻¹ followed by dissolved export in runoff, or depending on retentivity, adsorption onto fine-grained, reactive surfaces, typically clays and Fe- and Al-oxyhydroxides in soil horizons at the Earth's surface (Graly et al., 2010; Willenbring and von Blanckenburg, 2010). ¹⁰Be_{met} has been used as a tracer of Earth surface 35 processes, including estimating erosion rates at the soil-profile and river-catchment scales, soil residence times, ages of landforms over millennial to million-year timescales, and paleo-denudation rates from marine sedimentary records (Pavich et al., 1986; McKean et al., 1993; Jungers et al., 2009; Willenbring and von Blanckenburg, 2010; von Blanckenburg et al., 2012; von Blanckenburg and Bouchez, 2014; Wittman et al., 2015; von Blanckenburg et al., 2015; Portenga et al., 2019; Jelinski et al., 2019). Prerequisites for interpreting the concentrations and isotope ratios (i.e. ¹⁰Be_{met}/⁹Be) as erosion or 40 denudation (the sum of erosion and weathering) rates, respectively, include knowing the delivery rate of ¹⁰Be_{met} (Payich et al., 1986; Reusser et al., 2010; Graly et al., 2011; Heikkilä and von Blanckenburg, 2015; Dixon et al., 2018, Deng et al., 2020) and quantifying the mobility or retention of beryllium in soils (e.g. Bacon et al., 2012; Boschi and Willenbring, 2016a,b; Maher and von Blanckenburg, 2016; Dixon et al., 2018), not all of which was possible in many previous studies. The potential ability of using ¹⁰Be_{met} depth profiles to obtain quantitative data on soil ages, residence times, production- and denudation rates in a similar manner as in situ-produced ¹⁰Be (¹⁰Be_{in situ}) depth profiles could prove to be highly 45 advantageous, as it is easier to measure (due to much higher concentrations than ¹⁰Be_{in situ}) and can be employed in a much wider range of environments, as there is no dependence on the existence of coarse-grained quartz as is required for the analysis of ¹⁰Be_{in situ}. ¹⁰Be_{in situ} shares a cosmic ray origin with ¹⁰Be_{met} but differs in production method; ¹⁰Be_{in situ} is produced within crystal lattices in surface rocks and soil, rather than in the atmosphere, with a well constrained total production rate of 4.01 atoms g⁻¹y⁻¹ at sea level, high latitude (Borchers et al., 2016), and is characterized by full retentivity and known production pathways with depth. ¹⁰Be_{met}, in stark contrast, is potentially subjected to variable adsorption depths, incomplete retentivity, and heterogeneous internal redistribution.

In this study, we compare the previously published ¹⁰Be_{in situ} depth profiles of the Pinedale and Bull Lake terminal glacial moraines in Wind River, Wyoming (Schaller et al., 2009a,b) with new ¹⁰Be_{met} concentrations from depth profiles from the same sample material to evaluate the long-term (i.e. millennial) delivery rate of ¹⁰Be_{met} (F(¹⁰Be_{met})) to this site. This is the first study that evaluates F(¹⁰Be_{met}) for eroding soils as derived from the comparison of ¹⁰Be_{in situ} and ¹⁰Be_{met} depth profiles and erosion rates. We utilize previous knowledge of effective transient erosion rates from Schaller et al. (2009a), recalculated with revised parameters for *in situ* production of ¹⁰Be, to constrain and locally calibrate F(¹⁰Be_{met}) to these moraines while considering the extent of ¹⁰Be_{met} retention post-delivery. We then compare the resulting calculated F(¹⁰Be_{met}), with propagated uncertainties, with the predicted F(¹⁰Be_{met}) of Graly et al. (2011) and Heikkilä and von Blanckenburg (2015), normalizing each result for paleomagnetic field intensity variations over the Holocene. We also explore the practical differences between these flux estimates and advocate for each approach to be carried out when estimating F(¹⁰Be_{met}) for use in erosion rate calculations in future studies.

65 2 Background

70

2.1 Study Area

The Fremont Lake area of the Wind River Mountains (Wyoming, United States) experienced multiple glacial advances during the Pleistocene, evidenced by several moraines of Pinedale and Bull Lake age (Fig. 1; modified from original mapping and descriptions by Richmond, 1973). The climate is cold, semi-arid, and windy, with a 50-year precipitation rate and temperature of 27.6 cm y⁻¹ and 2.1° C, respectively (WRCC, 2005), in the nearby town of Pinedale, Wyoming (~3.5 km southwest of the field area).

The Pinedale and Bull Lake age terminal moraines (hereafter referred to as Pinedale and Bull Lake moraines) analyzed in this study (Fig. 1) were formed by highland-to-valley mountain glaciers draining an ice cap accumulation zone that covered the mountain range. The Pinedale moraine is more steep-sided and boulder-strewn than the gently sloping Bull Lake

moraine, each with a total height of \sim 30 m (see Figs. 1b, 1c of Schaller et al., 2009a for detailed moraine transects). The pH of the moraine soils is well characterized; both profiles have pedogenic carbonate below 1 m, fixing the pH at depth to \sim 8 (Chadwick and Chorover, 2001). Hall and Shroba (1995) report pH data on profiles adjacent to those analyzed in this study, with average pH ranging from \sim 5.5 on the surface to \sim 8 at depth.

80

85

90

95

The depth profile samples analyzed for 10 Be_{met} reported here are the same sample material analyzed for 10 Be_{in situ} by Schaller et al. (2009a). We utilize bulk samples sieved to <2 mm for our analysis, extracted from the lower mineral soil developed on each moraine, both mixtures of reworked glacial till (composed of Archean granite, granodiorite, and dioritic gneiss) that have a high likelihood for inheritance from cosmic ray exposure prior to burial. The same reported depths and grain size distributions apply for each sample at depth. The primary mineral content in the deepest (unweathered, >2 mm size fraction) sample is (in order of decreasing abundance): plagioclase, quartz, biotite, K-feldspar, hornblende, and magnetite (Taylor and Blum, 1995). Secondary clay minerals in the <2 μ m size fraction include kaolinite, vermiculite, illite, and smectite (Mahaney and Halvorson, 1986), with total clay content ranging from 3 to 10 wt% and 9 to 30 wt% for the Pinedale and Bull Lake profiles, respectively. Major element data is reported in Schaller et al. (2009b). Sr isotope measurements of the moraine soils and dust sources showed insignificant dust fluxes in the depth profiles of the Pinedale and Bull Lake moraines (Blum and Erel, 1997; Taylor and Blum, 1997).

2.2 Independent ¹⁰Be_{met} Flux Estimation

Accurately estimating $F(^{10}Be_{met})$ from field experiments is a topic of ongoing debate (e.g. Ouimet et al., 2015; Dixon et al., 2018), particularly in regard to the effect of precipitation rate on the flux (i.e. whether precipitation leads to additive or dilution effects on delivered $^{10}Be_{met}$, see *Willenbring and von Blanckenburg (2010)* and *Deng et al. (2020)* for extensive reviews). $F(^{10}Be_{met})$ also varies through time, depending on solar modulation and paleomagnetic field intensity, and has a spatial distribution primarily resulting from atmospheric mixing and scavenging. One means to estimate $^{10}Be_{met}$ production and delivery are $F(^{10}Be_{met})$ estimates based on global atmospheric models (Field et al., 2006; Heikkilä and von Blanckenburg, 2015), which provide an estimate over large spatial scales. Another type of estimate is based on empirical, precipitation-

dependent field estimates of ¹⁰Be_{met} inventories in dated soils (Graly et al., 2011) measured over annual time scales. The work of Ouimet et al. (2015) highlighted the necessity for local F(¹⁰Be_{met}) estimates that also integrate over millennial time scales against models such as these, as their comparison of ¹⁰Be_{met} inventories and deposition rates from Pinedale- and Bull Lake-aged landforms in the Colorado Front Range showed that some were lower, and some exceeded, deposition rates from atmospheric models and precipitation collections.

105

110

115

120

The F(10Be_{mat}) map of Heikkilä and von Blanckenburg (2015) utilizes the 10Be_{met} production functions of Masarik and Beer (1999) combined with the ECHAM5 general circulation model (GCM). Production rates were scaled to reflect the solar modulation and magnetic field strength for the entire Holocene (280.94 MV) using measured ¹⁰Be concentrations in ice cores. The authors ultimately present a global grid of predicted "pre-industrial" and "industrial" (referring to simulated aerosol and greenhouse gas concentrations) Holocene $F_{(^{10}Be_{met})}$ with an approximate cell size of 300 km x ~230 km. GCMs such as this are useful for modeling atmospheric mixing of ¹⁰Be_{met}, particularly in the stratosphere, as well as the regional effect of climate and its influence on $F(^{10}Be_{met})$ via atmospheric circulation and precipitation (Heikkilä et al., 2012). At this latitude (~42.9° N), the pre-industrial predicted $F_{(^{10}Be_{met})}$ of 1.38 x 10^6 atoms cm⁻² y⁻¹ is nearly identical to that derived from the flux map of Field et al. (2006), which utilizes the GISS (Goddard Institute for Space Studies Model E) GCM to model production. We use the pre-industrial modeled $F(^{10}Be_{met})$ in our comparisons, as it is a more appropriate estimate for landforms of these ages. To place an upper bound uncertainty on this estimate, which is otherwise hard to quantify, we utilize the difference between the industrial and pre-industrial predicted $F_{(^{10}\text{Be}_{met})}$ (+0.99 x 10^6 atoms cm⁻² y⁻¹). This difference is solely a result of climate-dependent shifts in the delivery of ¹⁰Be_{met} and shifts resulting from large industrial aerosol loading in modern times and does not reflect changes in atmospheric production (Heikkilä and von Blanckenburg, 2015).

On the other hand, the empirical, present-day estimates of F($^{10}Be_{met}$) from Graly et al. (2011) are based on measurements of $^{10}Be_{met}$ deposition rates from contemporary measurements of $^{10}Be_{met}$ in precipitation, corrected for dust and normalized to a modern (1951-2004) solar modulation value (700 MV). A first order estimate of the F($^{10}Be_{met}$) was empirically derived given latitude (L) and average precipitation rate (P) to the study area (Graly et al., 2011):

$$F(^{10}Be_{met}) = P \times (1.44 / (1 + EXP((30.7 - L) / 4.36)) + 0.63)$$
(1)

Uncertainty for this type of estimate can be determined using the root mean square error (1.75 x 10^3 atoms cm⁻³) of the resultant latitudinal trend in predicted $F(^{10}Be_{met})$ (see Fig. 5 of Graly et al., 2011). A predicted $F(^{10}Be_{met})$ of 0.55 (\pm 0.05) x 10^6 atoms cm⁻² y⁻¹ is calculated for these Wind River moraines using (Eq. 1), however in order to compare these two estimates with each other, as well as to our calculated $F(^{10}Be_{met})$, we later normalize them all to a common paleomagnetic and solar intensity datum (i.e. the Holocene).

3 Methods

140

135 3.1 Recalculating Previous Age Constraints

Ages for each moraine have been independently determined via multiple methods, with ¹⁰Be_{in situ} surface exposure ages of boulders combined with ²³⁰Th/U ages of nearby contemporaneous fluvial terraces yielding the most reliable average estimates of 21 ky and 140 ky for the Type-Pinedale and Bull Lake-age moraines, respectively (Gosse et al., 1995; Phillips et al., 1997; Easterbrook et al., 2003; Sharp et al., 2003). These ages closely correspond with global maximum ice volumes of marine oxygen isotope stages 2 and 6, respectively (Sharp et al., 2003). We recalculated the ¹⁰Be boulder surface exposure ages used to constrain the timing of advancement of each moraine to its terminal position based on a recent revision of the ¹⁰Be half-life, which affected the AMS standard values (Chmeleff et al., 2010), and the most recent nucleonic production rate of 3.92 atoms g⁻¹ y⁻¹ at sea level-high latitude (Borchers et al., 2016) (Table S1); the updated independent age constraints are 25 ky for the Pinedale moraine and remain at 140 ky for the Bull Lake moraine (see Supplementary Material for details).

3.2 Recalculating Previous Denudation Constraints

145

165

All moraine surfaces have been eroded to some extent after their deposition. To estimate the amount of erosion for our calculations, we utilize the previously reported denudation rates (comprising erosion and chemical loss by dissolution) for the Pinedale and Bull Lake moraines (Schaller et al., 2009a) from the same depth profiles and material analyzed in this study. The denudation rates of Schaller et al. (2009a) were calculated using a sea level, high latitude production rate of 5.1 atoms $g_{(017)}^{-1}$ v⁻¹ (Stone, 2000) and a decay constant of 4.62 x 10⁻⁷ v⁻¹. Denudation rates were recalculated using CRONUS 150 v.3 (Phillips et al., 2016) with the updated half-life and production rate values (Table S1) and updated independent age constraints scaled to the sample altitude and latitude (Dunai, 2000) assuming two denudation rate scenarios: one of constant denudation since moraine deposition, and the other of transient denudation decreasing in magnitude since moraine deposition. Recalculated average denudation rates are 32.1 ± 2.7 mm ky⁻¹ and 12.4 ± 4.8 mm ky⁻¹ for the Pinedale and Bull Lake moraines, respectively, in the case of transient denudation, and are 15 mm ky⁻¹ and 7.5 mm ky⁻¹ for the Pinedale and 155 Bull Lake moraines, respectively, in the case of constant denudation (Table 1). These recalculated denudation rates are determined from the best-fit Chi-Square solutions obtained from running Models 2, 4, 6, and 8 of Schaller et al. (2009a) with present-day parameters (See Supplementary Material for details). We consider the transient denudation rates to more closely approximate reality, as moraines, deposited as ~triangular landforms at the terminus of glaciers, initially experience faster 160 denudation than that towards present day, where the moraines evolve to a concave-down parabolic geometry. As the curvature of the topography reduces over time, hillslope diffusion law dictates that the denudation rates will decrease as the moraine flattens. This approach integrates this transient behavior over the entire age of each moraines, and thus likely overstates the loss of ¹⁰Be to erosion to some degree, however it nonetheless provides the most realistic estimates possible for these moraines as we are otherwise unable to independently constrain their site-specific erosion rates.

To properly compare the transient denudation rates of Schaller et al. (2009a) with the ¹⁰Be_{met}—derived erosion rates using the methods of von Blanckenburg et al. (2012), the weathering component of denudation must be accounted for. For the Pinedale moraine, chemical weathering mass loss is estimated to be 16% of the denudation rate, while for the Bull Lake

loss took place beneath the cosmic ray attenuation pathway, the recalculated average effective transient erosion rates are then 27.0 mm ky⁻¹ and 9.9 mm ky⁻¹ for the Pinedale and Bull Lake moraines, respectively. As we have no means to assess whether this assumption is correct, we instead account for this degree of potential loss in the uncertainties (in addition to analytical uncertainties) on the effective transient erosion rates in all further calculations. Regardless, we note that such weathering mass loss does not necessarily need to coincide with loss of dissolved ¹⁰Be_{met}. Rather, the sites of primary mineral dissolution might also be the sites of secondary mineral formation and high dissolved Ca ensuing circumneutral pH and hence potentially high ¹⁰Be_{met} retentivity.

3.3 10 Bemet Analysis

180

185

190

We analyzed approximately 1-2 g aliquots of the <2 mm grain-size moraine sediment fraction from the same ~10-15 cm depth intervals as Schaller et al. (2009a) analyzed for Be isotope abundance at the Laboratory for the Geochemistry of the Earth Surface at GFZ Potsdam. We followed the sediment leaching procedure described in Ebert et al. (2012) and Wittmann et al. (2012), which was adapted from Bourlés (1988) and Guelke-Stelling and von Blanckenburg (2012), to extract Be isotopes from outer grain surfaces. Bulk samples underwent two steps to remove the adsorbed beryllium: a 24-hr agitation in 0.5 M HCl (to extract amorphous oxide-bound Be), and 1 M hydroxylamine-hydrochloride (to remove crystalline-bound Be). After each step, the supernate was separated from the sediment.

To measure the adsorbed 10 Be_{met}, the two aliquots of leached material were combined and homogenized with ~200 µg of 9 Be carrier (Table 2) and 2 mL HF was added to the acid sample solution. This solution was nearly completely dried down and then dissolved in 1 additional mL of 50% HF acid and dried down completely, repeated once. We then added 10 mL ultrapure (18 M Ω) water to the warm fluoride residue and leached it for 1 h on a warm hotplate. The water containing the Be was gently removed via pipette and dried down separately. The Be in the water leach solution was extracted and purified by a form of the ion exchange chromatography procedure from von Blanckenburg et al. (2004) that was adapted for 10 Be_{met} purification by passing the leachate through anion (2 ml of BioRad 1x8 100-200 mesh resin) and cation (2x 1 ml BioRad AG50-X8 200-400 mesh) exchange resins, precipitated at pH ~9 using NH₄OH:H₂O (1:1), washed twice with 2 ml ultrapure water with centrifugation in between, mixed with AgCl, centrifuged and dried overnight, and finally oxidized over open

flame (>1000 °C; modified from Kohl & Nishiizumi, 1992). 10 Be_{met}/ 9 Be ratios were measured at the Zurich AMS Lab (Kubik and Christl, 2010) (S555 standard, nominal 10 Be/Be = 95.5 x $^{10-12}$), from which the 10 Be concentration (10 Be_{reac} = 10 Be_{met}) was calculated. Two carrier blanks analyzed with the samples register AMS 10 Be/ 9 Be ratios of $3.2 \pm 1.5 \times 10^{-15}$, and $2.2 \pm 1.5 \times 10^{-15}$ containing <0.1% of the 10 Be in analyzed samples.

3.4 10 Bemet Flux Calculations

In an actively eroding setting, erosion rates can be calculated with knowledge of 1) the total inventory of ¹⁰Be_{met} in the depth profile, 2) a known/estimated ¹⁰Be_{met} flux to the location, 3) the ¹⁰Be_{met} retention behavior, and 4) an assumption of approximate steady state conditions, which is only justified if the inventory of ¹⁰Be_{met} is independent of the initial exposure age of the soil. Here, steady state means that ¹⁰Be_{met} lost through erosion and decay equals the ¹⁰Be_{met} gained from atmospheric flux (e.g. Brown et al., 1988; Willenbring and von Blanckenburg, 2010), a prerequisite of which is that the residence time of soil material containing ¹⁰Be_{met} with respect to erosion is much less than the depositional age (Willenbring and von Blanckenburg, 2010), which holds true for these moraines. For an assumed steady state inventory, the inverse relationship between the local erosion rate and the ¹⁰Be_{met} content in the soil profile is exploited to determine a flux of ¹⁰Be_{met} using the formulation of Brown (1987), rearranged as follows:

210
$$F(^{10}Be_{met}) = E \times ([^{10}Be]_{reac} - [^{10}Be]_{inher}) + I\lambda$$
 (2)

Where E is the erosion rate [g cm⁻² y⁻¹], F(¹⁰Be_{met}) is the atmospheric flux of ¹⁰Be_{met} [atoms cm⁻² y⁻¹], [¹⁰Be]_{inher} is the inherited nuclide concentration [atoms cm⁻²], I is the inheritance-corrected inventory of ¹⁰Be_{met} [atoms cm⁻²] in the depth profile, λ is the decay constant of ¹⁰Be [y⁻¹], [¹⁰Be]_{reac} is the ¹⁰Be_{met} concentration at the surface of the soil [atoms g⁻¹]. Inventories were calculated following Willenbring and von Blanckenburg (2010) using a depth-averaged regolith density (ρ) of 2.0 g cm⁻³ for each profile (Schaller et al., 2009a,b), where z is the depth to the bottom of the soil column and ([¹⁰Be]_{reac}(z) - [¹⁰Be]_{inher}) is the concentration of ¹⁰Be_{met} at depth, minus inheritance:

220 $I = \int_0^z ([^{10}Be]_{reac}(z) - [^{10}Be]_{inher})\rho dz$ (3)

Both ¹⁰Be_{met} and ¹⁰Be_{in situ} depth profiles show indications of inherited nuclide concentrations at depth, likely due to incomplete glacial erosion resetting for each moraine (Schaller et al., 2009a) and exposure to ¹⁰Be_{met} during or immediately after glacial processes. Higher concentrations at depth are observed for the Bull Lake moraine for both nuclide profiles (Fig. 1, Table 2), potentially due to the presence of pre-irradiated reworked till. We consider the lowest concentration observed for each depth profile as [¹⁰Be]_{inher} and subtract it from all measured concentrations.

Desorption of ¹⁰Be_{met} can affect the inventory of ¹⁰Be_{met} when erosion rates are low, water flux is high and soil chemistry favors mobility. Given that for these soil profiles pH ranges from 8 at depth to ~5.5 at the surface (Hall and Shroba, 1995), we must consider incomplete retention of beryllium and thus a reduced inventory and surface concentration used in (Eq. 2) (Bacon et al., 2012; Maher and von Blanckenburg, 2016). Applying a correction directly to the calculation of ¹⁰Be_{met} flux is possible via a combination of (Eq. 2) (this study) and (Eq. 3) of von Blanckenburg et al. (2012), which requires an accurate estimation of the water flux out of the system (Q) and the Be partition coefficient (K_d).

235
$$F(^{10}Be_{met}) = E \times ([^{10}Be]_{reac} - [^{10}Be]_{inher}) + I\lambda + Q \times ([^{10}Be]_{reac} - [^{10}Be]_{inher}) \div K_d$$
 (4)

 K_d is estimated as 1 x 10⁵ to 1 x 10⁶ L kg⁻¹ (with an average of 5.5 x 10⁵ L kg⁻¹) from the surficial pH of ~5.5 to ~8 at depth via Be sorption-desorption experiments from You et al. (1989). We estimate Q by proxy via the modern precipitation rate of 276 L m⁻² y⁻¹.

240

Utilizing (Eq. 4) and previous knowledge of the effective transient erosion rates, we calculate the loss-corrected $F(^{10}Be_{met})$ to the locations of these moraines. To further account for the full range of possible K_d values and transient erosion rates, we use traditional algebraic error propagation to determine the uncertainty of the calculated fluxes.

3.6 Normalizing flux estimates for cosmic ray intensity variations over the Holocene

245 Geomagnetic field strength has varied considerably from the late Pleistocene to present and exerts the primary quantifiable influence on temporal variability in the production rate of cosmogenic nuclides in an inverse fashion (Pigati and Lifton. 2004). Relative paleointensity over the last 140 ky is, on average, ~20-40% less than the current geomagnetic intensity depending on the methodology employed (e.g. Frank et al., 1997; Valet et al., 2005). The flux map of Heikkilä and von Blanckenburg (2015) accounts for paleomagnetic field and solar intensity variations over the Holocene via the reconstruction 250 method of Steinhilber et al. (2012), which effectively increases the production rate used in their model by 1.23 times the present-day rate by rescaling the modern solar modulation factor (500 MV) and associated geomagnetic field intensity to that of the Holocene average (280.94 MV). As the estimations of flux from Graly et al. (2011) were normalized to reflect a solar modulation of 700 MV, we rescaled the modern Graly-derived $F_{(^{10}Be_{mel})}$ to the average Holocene solar modulation factor of 280.94 MV used in the flux map of Heikkilä and von Blanckenburg (2015) following the paleomagnetic and solar intensity 255 normalization procedure of Deng et al. (2020). This is carried out by first rescaling production at 700 MV to 500 MV (i.e. the modern solar modulation factor of Steinhilber et al., 2012) via Fig. 4B of Masarik & Beer (2009) for a Graly et al. (2011)-specific modern production ratio of 0.82 (Table 3). Then, to properly normalize for the Holocene, we multiply this modern production ratio by the reciprocal of the rescaling production ratio of Heikkilä and von Blanckenburg (2015) (1.23) to arrive at a Holocene-normalized production ratio of 0.67 and apply this to the Graly et al. (2011) flux estimate (Table 3). 260 We illustrate and further describe the details of this procedure in the Supplementary Material (Fig. S1).

To further compare the model- and the precipitation-derived Holocene-average $F(^{10}Be_{met})$ estimates with those calculated in this study, we must also normalize for geomagnetic and solar intensity variations within the Holocene (for Pinedale, with a 6 ky cosmogenic integration time) and beyond the Holocene (for Bull Lake, with a 24 ky cosmogenic integration time). We again linearly rescaled our calculated loss-corrected $F(^{10}Be_{met})$ for the Pinedale and Bull Lake moraines by first integrating the production rate relative to the modern using the Principle Component 1 (PC1) of the ^{10}Be marine core record of Christl et al. (2010), converting PC1 into relative fluxes from 6 ky and 24 ky, respectively, and then normalizing these values to those over the Holocene, propagating the statistical uncertainties. These time intervals represent the calculated

residence/integration times of the soil profiles from the surface to the e-folding adsorption depth of 10 Be_{met} (20 and 30 cm for the Pinedale and Bull Lake moraines, respectively). This approach accounts for the cumulative effects of transient erosion and leaching by weighting geomagnetic intensity variations on $F_{(^{10}\text{Be}_{met})}$ towards the present.

4 Results

270

4.1 Meteoric Cosmogenic ¹⁰Be Concentrations

The measured ¹⁰Be_{met} concentrations are reported along with the previously published ¹⁰Be_{in situ} concentrations (Schaller et al., 2009a) for the Pinedale and Bull Lake profiles (Table 2); ¹⁰Be_{met} depth profiles are presented for the Pinedale and Bull Lake profiles in Figure 2. The Pinedale depth profile has ¹⁰Be_{met} concentrations ranging from 3.57 (± 0.32) to 199.53 (± 5.26) x 10⁶ atoms g⁻¹. The highest nuclide concentration is measured at 10 cm, rather than at the surface. Below this maximum value, concentrations decrease exponentially until reaching an asymptote at ~ 3 to 6 x 10⁶ atoms g⁻¹ from 43 cm to the bottom of the profile (180 cm), the lowest of which we consider to be an inherited component. The Pinedale depth profile has a calculated, inheritance-corrected inventory (Eq. 3) of 5387 (± 122) x 10⁶ atoms cm⁻².

The Bull Lake depth profile has 10 Be_{met} concentrations ranging from 6.32 (\pm 0.25) to 415.48 (\pm 12.46) x 106 atoms g⁻¹. The highest nuclide concentration is measured at the surface; below this, concentrations decrease in an approximately exponential fashion until reaching an asymptote at \sim 6 to 8 x 106 atoms g⁻¹ from 64 cm to the bottom of the profile (130 cm), the lowest of which we also consider to be an inherited component. The Bull Lake depth profile has a calculated, inheritance-corrected inventory (Eq. 3) of 17310 (\pm 318) x 106 atoms cm⁻². The 10 Be_{met} inventory from the Bull Lake moraine is roughly 3 times higher than that of the Pinedale moraine.

4.2 ¹⁰Bemet Fluxes

285

The loss-corrected $F_{(^{10}Be_{met})}$ as calculated from (Eq. 4) is 1.04 (± 0.14) x 10⁶ atoms cm⁻² y⁻¹ and 1.04 (± 0.39) x 10⁶ atoms cm⁻² y⁻¹ for the Pinedale and Bull Lake moraines, respectively (Table 3), with uncertainties determined via traditional algebraic error propagation, assuming a Gaussian distribution for the estimated K_d and transient erosion rate values.

Retention calculations from (Eq. 4) across the entire range of possible K_d values indicate that the potential desorption loss at the surface of the Pinedale and Bull Lake profiles ranges from 0.4% to 3.6% and 0.9% to 8.9%, respectively. The average calculated loss (reported above) compared to calculations without considering retention is 0.8% and 2.0% for the Pinedale and Bull Lake profiles, respectively.

These loss-corrected calculated fluxes are then normalized for paleomagnetic field intensity variations over the Holocene and compared in order to evaluate the $F(^{10}Be_{met})$ to this area. The Holocene-average loss-corrected $F(^{10}Be_{met})$ from this study are $1.46 (\pm 0.20) \times 10^6$ atoms cm⁻² y⁻¹ and $1.30 (\pm 0.48) \times 10^6$ atoms cm⁻² y⁻¹ for the Pinedale and Bull Lake moraines, respectively (Table 3).

The predicted Holocene-average $F(^{10}Be_{met})$ of Graly et al. (2011) for this site is 0.83 (± 0.08) x 10⁶ atoms cm⁻² y⁻¹ (Table 3). As the pre-industrial flux map of Heikkilä and von Blanckenburg (2015) already presents a Holocene-average $F(^{10}Be_{met})$ of 1.38 (+ 0.99) x 10⁶ atoms cm⁻² y⁻¹, no normalization for this method needs to be carried out.

5 Discussion

300

310

315

5.1 Cosmogenic Nuclide Profiles

This trend can be explained most simply by the reactive transport of dissolved ¹⁰Be_{met} with infiltrating water (e.g. Willenbring and von Blanckenburg, 2010), as exponential ¹⁰Be_{met} profiles are predicted by reactive transport models (Maher and von Blanckenburg, 2016).

An approximately exponential decrease in ¹⁰Be_{met} with depth is observed for the Pinedale and Bull Lake moraines (Fig. 2).

The maximum ¹⁰Be_{met} concentration for the Pinedale moraine is measured at 10 cm depth, rather than the most surficial sample (3 cm). This peak concentration corresponds with the clay rich layer of the B-horizon in the soil profile (Table 2). This potentially indicates that this layer acts as a zone of illuviation, often observed in soil profiles that contain a mid-depth

clay-rich horizon (e.g. Monaghan et al., 1992) formed by vertical transport of soil particles containing ¹⁰Be_{met} (Jagercikova et al., 2016). This subsurface maximum could be the result of smaller grain sizes within this horizon, as these grains have a higher surface area per unit mass and can exchange ions more easily (Brown et al., 1992; Willenbring and von Blanckenburg, 2010). Alternatively, enhanced ¹⁰Be_{met} incorporation into the lattices of newly formed clays and oxyhydroxides at depth (e.g. Barg et al., 1997) might explain this maximum. This phenomenon is not observed for the Bull Lake moraine; the highest clay content observed in the profile is in the Bk-horizon at a depth of 43 cm (Schaller et al., 2009a,b), however no increase or anomalous high ¹⁰Be_{met} concentration is observed (Fig. 2, Table 2). It is possible that such an increase may have been missed in the Bull Lake profile, as the equivalent 10 cm depth interval was not sampled.

Peculiarly, the observed mixing depths for the Pinedale and Bull Lake moraines as determined from the ¹⁰Be_{in situ} depth 325 profiles of Schaller et al. (2009a) (~40 and 50 cm, respectively) are not observed for the ¹⁰Be_{met} depth profiles (Fig. 2). A couple of viable reasons for a lack of a mixing signal in the ¹⁰Be_{met} depth profiles exist. The different grain sizes analyzed here and in Schaller et al. (2009a) might exhibit different diffusion coefficients, by which larger grain sizes are more easily mixed, however a trend in smaller grain size fractions with depth within the ¹⁰Be_{in situ} mixing layer would likely be observed 330 if this were the case. Unfortunately, separate grain size classes were not measured for ¹⁰Be_{in situ} within the full mixing zone of either profile to further assess this explanation. Another possibility is that the advection of ¹⁰Be_{met} from the surface swamps the effect of mixing that is apparent in the ¹⁰Be_{in situ} depth profiles. This could indicate that continual ¹⁰Be_{met} delivery and reactive flow resets the ¹⁰Be_{met} profile at timescales much shorter than that of physical mixing. Profiles with a relatively low surficial pH (<5) might be particularly susceptible to this phenomenon due to incomplete retention or differential mobility 335 of ¹⁰Be_{met} (Kaste and Baskaran, 2011), although the profiles analyzed here are not likely to show appreciable (>9%) ¹⁰Be_{met} loss at depth due to retention issues. Nonetheless, the formation of a clay horizon in the Pinedale moraine may indicate that soil horizonation happens more rapidly than soil mixing, as inferred from the ¹⁰Bein situ depth profile (Schaller et al., 2009a), suggesting that ¹⁰Be_{met} advection from the surface is a more likely explanation.

5.1.1 ¹⁰Be_{met} Retention

A range of possibilities exist for retention effects and associated surficial ¹⁰Be_{met} loss for these profiles. For the highest K_d estimate, at 1 x 10⁶ L kg⁻¹, potential loss is as low as 0.4% and 0.8% for the Pinedale and Bull Lake profiles, respectively. For an average K_d of 5.5 x 10⁵ L kg⁻¹, the potential loss is likewise negligible, at 0.8% and 2.0% for the Pinedale and Bull Lake profiles, respectively. On the other hand, for the lowest K_d estimate, at 1 x 10⁵ L kg⁻¹, ¹⁰Be_{met} loss due to desorption could be as great as 3.6% and 8.9% at the surface of the Pinedale and Bull Lake profiles, respectively. While the possibility of desorption cannot be ruled out, it's unlikely that either profile has experienced loss to such a degree, as pH, and thus K_d and retentivity, increases with depth. Even in the worst-case scenario of assuming maximum possible loss at the lowest K_d estimate, the magnitude of the potential loss does not substantially affect our calculated F(¹⁰Be_{met}) estimates within uncertainties. Our calculations thus capture the potential maximum bound for loss via propagated uncertainties.

5.2 ¹⁰Be_{met} flux estimation; sources of variability

The calculated, loss- and paleointensity-corrected F(10Bemet) of 1.46 (± 0.20) x 106 atoms cm⁻² y⁻¹ and 1.30 (± 0.48) x 106 atoms cm⁻² y⁻¹ for the Pinedale and Bull Lake moraines, respectively, are higher compared to that estimated by Graly et al. (2011), at 0.83 x 106 atoms cm⁻² y⁻¹, and agree within uncertainty with that predicted by Heikkilä and von Blanckenburg (2015), at 1.38 x 106 atoms cm⁻² y⁻¹ (Table 3). The considerable discrepancy between the predicted F(10Bemet) of each method arises primarily from differences in how each methodology treats the influence that precipitation rate has on the flux to a given area and, in particular for this study, how large of an area is covered. The 310 km x 228 km flux map grid cell of Heikkilä and von Blanckenburg (2015) covers the entirety of the Wind River Range and the surrounding, relatively lowlying flatlands (Fig. 1), where precipitation estimates vary considerably, by over an order of magnitude (WRCC, 2005), due to elevation and topographic effects on precipitation (Hostetler and Clark, 1997). For example, if one were to estimate F(10Bemet) from Graly et al. (2011) via (Eq. 1) to nearby Fish Lake Mountain contained within the same Heikkilä and von Blanckenburg (2015) grid cell as this study site, with a modern precipitation rate of 128 cm y⁻¹ (WRCC, 2005), the F(10Bemet) would be 2.5 x 106 atoms cm⁻² y⁻¹, substantially higher than that predicted from Heikkilä and von Blanckenburg (2015).

Considering this alone, it is not surprising that such a discrepancy exists between methods, nor is this a unique occurrence (e.g. Jungers et al., 2009; Schooneians et al., 2017; Dixon et al., 2018; Deng et al., 2020).

365 Each approach has its own set of shortcomings, precluding agreement between each approach in sites such as this. The flux map of Heikkilä and von Blanckenburg (2015) has a coarse resolution and does not handle short wavelength orographic effects well, along with being model based and requiring many assumptions on atmospheric scavenging. The formula of Graly et al. (2011), on the other hand, does not take atmospheric circulation into account, instead relying on data from sites with relatively high rates of precipitation to derive an empirical formula. Recent work by Deng et al. (2020) highlights the 370 potential for precipitation estimates to differ from GCM-derived estimates due to short timescale additive effects (sensu Willenbring and von Blanckenburg, 2010). Further, they find that in the majority of studies globally, GCM- and soil-derived $F_{(10_{\text{Be}_{\text{max}}})}$ estimates agree within a factor of two. That the calculated fluxes of this study agree with the GCM-modeled preindustrial $F(^{10}Be_{mot})$ of Heikkilä and von Blanckenburg (2015) provides further evidence of this general observation. In any event, the strength of future ¹⁰Be_{met} studies relies upon careful consideration of beryllium retention, spatial scale, and paleomagnetic intensity when determining $F(^{10}Be_{met})$. As calculating a long-term delivery rate of $F(^{10}Be_{met})$ for a particular site 375 using $^{10}\text{Be}_{\text{in situ}}$ and $^{10}\text{Be}_{\text{met}}$ is both costly and time-intensive, it is especially prudent to estimate $F(^{10}\text{Be}_{\text{met}})$ using both methods compared here for robust calculations utilizing $F(^{10}Be_{met})$ (e.g. $^{10}Be_{met}$ -derived erosion rates) in the future.

6. Conclusions

380

In this study, we compare new meteoric 10 Be (10 Be_{met}) and previously published *in situ*-produced 10 Be (10 Be_{in situ}) depth profile measurements from the well-characterized Pinedale (\sim 21-25 ky) and Bull Lake (\sim 140 ky) moraines of Wind River, Wyoming. Our ability to utilize previous knowledge of transient erosion rates from the 10 Be_{in situ} depth profile measurements of Schaller et al. (2009a), recalculated with revised parameters, allows us to calculate loss-corrected Holocene average 10 Be_{met} fluxes of 1.46 (\pm 0.20) x 10 6 atoms cm⁻² y⁻¹ and 1.30 (\pm 0.48) x 10 6 atoms cm⁻² y⁻¹ to the Pinedale and Bull Lake moraines, respectively. Comparing these fluxes to two independent estimation methods reveals that the empirical flux

estimate of Graly et al. (2011), after normalizing for Holocene paleomagnetic intensity, at 0.83 (± 0.08) x 10⁶ atoms cm⁻² y⁻¹, is lower than the calculated fluxes, and the modeled Holocene flux estimate of Heikkila and von Blanckenburg (2015), at 1.38 x 10⁶ atoms cm⁻² y⁻¹, agrees within uncertainty to the calculated fluxes. We find that loss of ¹⁰Be_{met} in these profiles due to pH-influenced mobility/dissolution effects exerts a relatively minor potential control (biasing from <1% up to 9% in the most extreme case) on flux calculations. Inspection of the ¹⁰Be_{met} depth profiles and their near-surface concentrations suggest that soil mixing to depths of 40 and 50 cm, as observed for the Pinedale and Bull Lake ¹⁰Be_{in situ} depth profiles, respectively, is not represented by the finer grain sizes analyzed in this study. The lack of a mixing signal may be most simply explained by a swamping effect from continual delivery and advection of ¹⁰Be_{met} from the surface that occurs over more rapid timescales than soil mixing. These differences in the depth-concentration relationships between ¹⁰Be_{met} and ¹⁰Be_{in situ} might open up a new area of research to study particle movement in soils.

Author Contribution

395

400

TC is a current Ph.D. student at Stanford University and conducted the majority of the work during 2018-2019 under the supervision of JWK, who contributed to several drafts of the original manuscript as well as preparation of the meteoric data set at GFZ Potsdam. MS and JDB contributed via ¹⁰Be data acquisition, interpretation, and discussion; MC and PWK contributed via AMS measurements at ETH-Zurich. FvB assisted in interpretation of the comparative data set and associated discussion of meteoric ¹⁰Be flux estimates, mobility/retention, and paleomagnetic field intensity normalization and contributed to manuscript drafts.

Competing Interests

The authors declare no competing interests for this manuscript.

Acknowledgement

This work was made possible through the German Science Foundation Grant *BL562*/7 and an Alexander von Humboldt Postdoctoral Fellowship. Support for TC came from a Career grant to Willenbring from NSF #1651243. The authors thank three anonymous reviewers for constructive comments and suggestions which greatly improved the manuscript.

References

- Bacon, A. R., Richter, D. D., Bierman, P. R., and Rood, D. H.: Coupling meteoric 10Be with pedogenic losses of 9Be to improve soil residence time estimates on an ancient North American interfluve, Geology, 40(9), 847-850, https://doi.org/10.1130/G33449.1, 2012
- Barg, E., Lal, D., Pavich, M. J., Caffee, M. W., and Southon, J. R.: Beryllium geochemistry in soils; evaluation of 10Be/9Be ratios in authigenic minerals as a basis for age models. Chemical Geology, 140, 237-258, https://doi.org/10.1016/S0009-2541(97)00051-X, 1997.
 - Blum, J. D., and Erel, Y.: Rb/Sr isotope systematics of a granitic soil chronosequence: The importance of biotite weathering, Geochimica et Cosmochimica Acta, 61(15), 3193-3204, https://doi.org/10.1016/S0016-7037(97)00148-8, 1997.
- Borchers, B., Marrero, S., Balco, G., Caffee, M., Goehring, B., Lifton, N., ... and Stone, J.: Geological calibration of spallation production rates in the CRONUS-Earth project, Quaternary Geochronology, 31, 188-198, https://doi.org/10.1016/j.quageo.2015.01.009, 2016.
- Bourlès, D.: Étude de la géochimie de l'isotope cosmogénique ¹⁰Be et de son isotope stable 9Be en milieu océanique: 425 application à la datation des sédiments marins, Ph.D. thesis, Université Paris XI, Centre d'Orsay, 1988.
 - Boschi, V., Willenbring, J.K.:The role of pH, organic matter composition and mineralogy on the sorption behavior of beryllium. Environmental Chemistry. http://dx.doi.org/10.1071/EN15107, 2016a.
- Boschi, V., Willenbring, J.K.: Beryllium Desorption from Minerals and Organic Ligands Over Time. Chemical Geology, 439(7) 52–58. http://dx.doi.org/10.1016/j.chemgeo.2016.06.009, 2016b.
 - Brown, L.: 10Be as a tracer of erosion and sediment transport. Chemical Geology: Isotope Geoscience section, 65(3-4), 189-196, https://doi.org/10.1016/0168-9622(87)90002-9, 1987.
- Brown, L., Pavich, M. J., Hickman, R. E., Klein, J., Middleton, R.: Erosion of the Eastern United States observed with 10Be. Earth Surface Processes and Landforms, 13, 441-457, https://doi.org/10.1002/esp.3290130509, 1988.
- Brown, E. T., Edmond, J. M., Raisbeck, G. M., Bourlès, D. L., Yiou, F., and Measures, C. I.: Beryllium isotope geochemistry in tropical river basins, Geochimica et Cosmochimica Acta, 56(4), 1607-1624, https://doi.org/10.1016/0016-7037(92)90228-B, 1992.
 - Chadwick, O. A., & Chorover, J., The chemistry of pedogenic thresholds, Geoderma, 100(3-4), 321-353, https://doi.org/10.1016/S0016-7061(01)00027-1, 2001.
- Chmeleff, J., von Blanckenburg, F., Kosser, K., and Jakob, D.: Determination of the 10Be half-life by multicollecter ICP-MS and liquid scintillation counting, Nuclear Instruments and Methods in Physics Research Section B: Beam Interactions with Materials and Atoms, 268(2), 192–199, https://doi.org/10.1016/j.nimb.2009.09.012, 2010.
- Christl, M., Lippold, J., Steinhilber, F., Bernsdorff, F., and Mangini, A.: Reconstruction of global 10Be production over the past 250 ka from highly accumulating Atlantic drift sediments, Quaternary Science Reviews, 29(19-20), 2663-2672, https://doi.org/10.1016/j.quascirev.2010.06.017, 2010.
- Deng, K., Wittmann, H., and von Blanckenburg, F.: The depositional flux of meteoric cosmogenic 10Be from modelling and observation, Earth and Planetary Science Letters, 550, 116530, https://doi.org/10.1016/j.epsl.2020.116530, 2020.

- Dixon, J. L., Chadwick, O. A., and Pavich, M. J.: Climatically controlled delivery and retention of meteoric 10Be in soils, Geology, 46(10), 899-902, https://doi.org/10.1130/G45176.1, 2018.
- Dunai, T. J.: Scaling factors for production rates of in situ produced cosmogenic nuclides: a critical reevaluation, Earth and Planetary Science Letters, 176(1), 157-169, https://doi.org/10.1016/S0012-821X(99)00310-6, 2000.
- Easterbrook, D. J., Pierce, K., Gosse, J., Gillespie, A., Evenson, E., and Hamblin, K.: Quaternary geology of the western United States, in: Quaternary Geology of the United States, edited by: Easterbrook, D. J., Desert Res. Inst., Reno, Nev., 19-79, 2003.
 - Ebert, K., Willenbring, J., Norton, K. P., Hall, A., and Hättestrand, C.: Meteoric 10Be concentrations from saprolite and till in northern Sweden: Implications for glacial erosion and age, Quaternary Geochronology, 12, 11-22, https://doi.org/10.1016/j.quageo.2012.05.005, 2012.
- Field, C. V., Schmidt, G. A., Koch, D., and Salyk, C.: Modeling production and climate-related impacts on 10Be concentration in ice cores, Journal of Geophysical Research: Atmospheres, 111(D15), https://doi.org/10.1029/2005JD006410, 2006.

- Frank, M., Schwarz, B., Baumann, S., Kubik, P. W., Suter, M., and Mangini, A.: A 200 kyr record of cosmogenic radionuclide production rate and geomagnetic field intensity from 10Be in globally stacked deep-sea sediments, Earth and Planetary Science Letters, 149(1-4), 121-129, https://doi.org/10.1016/S0012-821X(97)00070-8, 1997.
- Guelke-Stelling, M., and von Blanckenburg, F.: Fe isotope fractionation caused by translocation of iron during growth of bean and oat as models of strategy I and II plants, Plant and soil, 352(1-2), 217-231, https://doi.org/10.1007/s11104-011-0990-9, 2012.
 - Gosse, J. C., Klein, J., Lawn, B., Middleton, R., and Evenson, E. B.: Beryllium-10 dating of the duration and retreat of the last Pinedale glacial sequence, Science, 268(5215), 1329-1333, https://doi.org/10.1126/science.268.5215.1329, 1995.
- Graly, J. A., Bierman, P. R., Reusser, L. J., and Pavich, M. J.: Meteoric ¹⁰Be in soil profiles—a global meta-analysis, Geochimica et Cosmochimica Acta, 74(23), 6814-6892, https://doi.org/10.1016/j.gca.2010.08.036, 2010.
- Graly, J. A., Reusser, L. J., and Bierman, P. R.: Short and long-term delivery rates of meteoric 10Be to terrestrial soils, Earth and Planetary Science Letters, 302(3-4), 329-336, https://doi.org/10.1016/j.epsl.2010.12.020, 2011.
 - Hall, R. D., and Shroba, R. R.: Soil evidence for a glaciation intermediate between the Bull Lake and Pinedale glaciations at Fremont Lake, Wind River Range, Wyoming, USA, Arctic and Alpine Research, 27(1), 89-98, https://doi.org/10.2307/1552071, 1995.
 - Heikkilä, U. and Smith, A. M.: Influence of model resolution on the atmospheric transport of 10Be, Atmospheric Chemistry and Physics, 12(21), 10601-10612, https://doi.org/10.5194/acp-12-10601-2012, 2012.
- Heikkilä, U. and Von Blanckenburg, F.: The global distribution of Holocene meteoric 10Be fluxes from atmospheric models, GFZ Data Services, GFZ Potsdam, Germany, http://doi.org/10.5880/GFZ.3.4.2015.001, 2015.
 - Hostetler, S. W., and Clark, P. U.: Climatic controls of western US glaciers at the last glacial maximum, Quaternary Science Reviews, 16(6), 505-511, https://doi.org/10.1016/S0277-3791(96)00116-3, 1997.

- Jagercikova, M., Cornu, S., Bourlès, D., Evrard, O., Hatté, C. and Balesdent, J.: Quantification of vertical solid matter transfers in soils during pedogenesis by a multi-tracer approach, Journal of Soils and Sediments, 17, 408-422, https://doi.org/10.1007/s11368-016-1560-9, 2016.
- Jelinski, N., Willenbring, J.K., Schumacher, T.E., Li, S. Lobb, D.A., Papiernik, S.K., and Yoo, K.: Meteoric Beryllium-10 as a tracer of cumulative erosion due to post-settlement land use in west-central Minnesota, USA, Journal of Geophysical Research Earth Surface, 124(4), 874-901, https://doi.org/10.1029/2018JF004720, 2019.
 - Jungers, M. C., Bierman, P. R., Matmon, A., Nichols, K., Larsen, J., and Finkel, R.: Tracing hillslope sediment production and transport with in situ and meteoric 10Be, Journal of Geophysical Research: Earth Surface, 114(F4),
- 515 https://doi.org/10.1029/2008JF001086, 2009.
 - Kaste, J. M., and Baskaran, M.: Meteoric 7Be and 10Be as process tracers in the environment, in: Handbook of environmental isotope geochemistry, edited by: Baskaran, M., Springer, Berlin, Heidelberg, 61-85, https://doi.org/10.1007/978-3-642-10637-8 5, 2012.
- Kubik, P. W., and Christl, M.: 10Be and 26Al measurements at the Zurich 6 MV Tandem AMS facility, Nuclear Instruments and Methods in Physics Research Section B: Beam Interactions with Materials and Atoms, 268(7-8), 880-883, https://doi.org/10.1016/j.nimb.2009.10.054, 2010.
- Kohl, C. P., and Nishiizumi, K.: Chemical isolation of quartz for measurement of in-situ -produced cosmogenic nuclides, Geochimica et Cosmochimica Acta, 56(9), 3583-3587, https://doi.org/10.1016/0016-7037(92)90401-4, 1992.
 - Lal, D. and Peters, B.: Cosmic ray produced radioactivity on the Earth, in: Kosmische Strahlung II/Cosmic Rays II, edited by: Sitte, K., Springer, Berlin, Heidelberg, 551-612, https://doi.org/10.1007/978-3-642-46079-1_7, 1967.
- Mahaney, W. C., and Halvorson, D. L.: Rates of mineral weathering in the Wind River Mountains, western Wyoming, in: Rates of chemical weathering of rocks and minerals, edited by: Colman, S., and Dethier, D., Academic Press, Cambridge, Massachusetts, 147-167, 1986.
- Maher, K., and von Blanckenburg, F.: Surface ages and weathering rates from 10Be (meteoric) and 10Be/9 Be: insights from differential mass balance and reactive transport modeling, Chemical Geology, 446, 70-86, https://doi.org/10.1016/j.chemgeo.2016.07.016, 2016.
- Masarik, J., and Beer, J.: Simulation of particle fluxes and cosmogenic nuclide production in the Earth's atmosphere, Journal of Geophysical Research: Atmospheres, 104(D10), 12099-12111, https://doi.org/10.1029/1998JD200091, 1999.
 - Masarik, J., and Beer, J.: An updated simulation of particle fluxes and cosmogenic nuclide production in the Earth's atmosphere, Journal of Geophysical Research: Atmospheres, 114(D11), https://doi.org/10.1029/2008JD010557, 2009.
- Mckean, J.A., Dietrich, W.E., Finkel, R.C., Southon, J.R., and Caffee, M.W.: Quantification of Soil Production and Downslope Creep Rates from Cosmogenic Be-10 Accumulations on a Hillslope Profile, Geology, 21, 343-346, https://doi.org/10.1130/0091-7613(1993)021<0343:QOSPAD>2.3.CO;2, 1993.
- Monaghan, M. C., McKean, J., Dietrich, W., and Klein, J.: 10Be chronometry of bedrock-to-soil conversion rates, Earth and Planetary Science Letters, 111(2-4), 483-492, https://doi.org/10.1016/0012-821X(92)90198-5, 1992.

- Ouimet, W., Dethier, D., Bierman, P., Wyshnytzkyr, C., Shea, N., and Rood, D. H.: Spatial and temporal variations in meteoric 10Be inventories and long-term deposition rates, Colorado Front Range, Quaternary Science Reviews, 109, 1-12,
- 555 https://doi.org/10.1016/j.catena.2014.12.008, 2015.

- Pavich, M. J., Brown, L., Harden, J., Klein, J., and Middleton, R.: 10Be distribution in soils from Merced River terraces, California, Geochimica et Cosmochimica Acta, 50(8), 1727-1735, https://doi.org/10.1016/0016-7037(86)90134-1, 1986.
- Phillips, F. M., Zreda, M. G., Gosse, J. C., Klein, J., Evenson, E. B., Hall, R. D., Chadwick, O.A., and Sharma, P.: Cosmogenic 36Cl and 10Be ages of Quaternary glacial and fluvial deposits of the Wind River Range, Wyoming, Geological Society of America Bulletin, 109(11), 1453-1463, https://doi.org/10.1130/0016-7606(1997)109<1453:CCABAO>2.3.CO;2, 1997.
- Phillips, F. M., Argento, D. C., Balco, G., Caffee, M. W., Clem, J., Dunai, T. J., ... and Jull, A. T.: The CRONUS-Earth project: a synthesis, Quaternary Geochronology, 31, 119-154, https://doi.org/10.1016/j.quageo.2015.09.006, 2016.
 - Pigati, J. S. and Lifton, N. A.: Geomagnetic effects on time-integrated cosmogenic nuclide production with emphasis on in situ 14C and 10Be, Earth and Planetary Science Letters, 226(1-2), 193-205, https://doi.org/10.1016/j.epsl.2004.07.031, 2004.
- Portenga, E.W., Bierman, P.R., Trodick Jr, C.D., Greene, S.E., DeJong, B.D., Rood, D.H., and Pavich, M.J.: Erosion rates and sediment flux within the Potomac River basin quantified over millennial timescales using beryllium isotopes, GSA Bulletin, 131(7-8), 1295-1311, https://doi.org/10.1130/B31840.1, 2019.
- Reusser, L., Graly, J., Bierman, P., and Rood, D.: Calibrating a long-term meteoric 10Be accumulation rate in soil, Geophysical Research Letters, 37(19), https://doi.org/10.1029/2010GL044751, 2010.
 - Richmond, G. M.: Geologic map of the Fremont Lake south quadrangle, Sublette County, Wyoming, Map 1138, https://doi.org/10.3133/gq1138, 1973.
 - Schaller, M., Ehlers, T. A., Blum, J. D., and Kyrllenberg, M. A.: Quantifying glacial moraine age, denudation, and soil mixing with cosmogenic nuclide depth profiles, Journal of Geophysical Research: Earth Surface, 114(F1), https://doi.org/10.1029/2007JF000921, 2009a.
- Schaller, M., Blum, J. D., & Ehlers, T. A.: Combining cosmogenic nuclides and major elements from moraine soil profiles to improve weathering rate estimates, Geomorphology, 106(3-4), 198-205, https://doi.org/10.1016/j.geomorph.2008.10.014, 2009b.
- Schoonejans, J., Vanacker, V., Opfergelt, S., and Christl, M.: Long-term soil erosion derived from in-situ 10Be and inventories of meteoric 10Be in deeply weathered soils in southern Brazil. Chemical Geology, 466, 380-388, https://doi.org/10.1016/j.chemgeo.2017.06.025, 2017.
- Sharp, W. D., Ludwig, K. R., Chadwick, O. A., Amundson, R., and Glaser, L. L.: Dating fluvial terraces by 230 Th/U on pedogenic carbonate, Wind River Basin, Wyoming, Quaternary Research, 59(2), 139-150, https://doi.org/10.1016/S0033-5894(03)00003-6, 2003.
 - Steinhilber, F., Abreu, J. A., Beer, J., and McCracken, K. G.: Interplanetary magnetic field during the past 9300 years inferred from cosmogenic radionuclides, Journal of Geophysical Research: Space Physics, 115(A1), https://doi.org/10.1029/2009JA014193, 2010.
 - Stone, J. O.: Air pressure and cosmogenic isotope production, Journal of Geophysical Research: Solid Earth, 105(B10), 23753-23759, https://doi.org/10.1029/2000JB900181, 2000.

- Taylor, A. and Blum, J. D.: Relation between soil age and silicate weathering rates determined from the chemical evolution of a glacial chronosequence, Geology, 23(11), 979-982, https://doi.org/10.1130/0091-7613(1995)023<0979:RBSAAS>2.3.CO;2, 1995.
 - Taylor, A. and Blum, J. D.: Relation between soil age and silicate weathering rates determined from the chemical evolution of a glacial chronosequence: Reply, Geology, 25(4), 382-383, 1997.
- Valet, J. P., Meynadier, L., and Guyodo, Y.: Geomagnetic dipole strength and reversal rate over the past two million years, Nature, 435(7043), 802-805, https://doi.org/10.1038/nature03674, 2005.

630

- von Blanckenburg, F., Hewawasam, T., and Kubik, P. W.: Cosmogenic nuclide evidence for low weathering and denudation in the wet, tropical highlands of Sri Lanka, Journal of Geophysical Research: Earth Surface, 109(F3), https://doi.org/10.1029/2003JF000049, 2004.
 - von Blanckenburg, F., Bouchez, J., and Wittmann, H.: Earth surface erosion and weathering from the 10Be (meteoric)/9Be ratio, Earth and Planetary Science Letters, 351, 295-305, https://doi.org/10.1016/j.epsl.2012.07.022, 2012.
- von Blanckenburg, F., and Bouchez, J.: River fluxes to the sea from the ocean's 10Be/9Be ratio. Earth and Planetary Science Letters, 387, 34-43, https://doi.org/10.1016/j.epsl.2013.11.004, 2014.
- von Blanckenburg, F., Bouchez, J., Ibarra, D.E., and Maher, K.: Stable runoff and weathering fluxes into the oceans over Quaternary climate cycles, Nature Geoscience, 8, 538-U146, https://doi.org/10.1038/ngeo2452, 2015.
 - Willenbring, J. K., and von Blanckenburg, F.: Meteoric cosmogenic Beryllium-10 adsorbed to river sediment and soil: Applications for Earth-surface dynamics. Earth-Science Reviews, 98(1-2), 105-122, https://doi.org/10.1016/j.earscirev.2009.10.008, 2010.
 - Wittmann, H., Von Blanckenburg, F., Bouchez, J., Dannhaus, N., Naumann, R., Christl, M., and Gaillardet, J.: The dependence of meteoric 10Be concentrations on particle size in Amazon River bed sediment and the extraction of reactive 10Be/9Be ratios, Chemical Geology, 318, 126-138, https://doi.org/10.1016/j.chemgeo.2012.04.031, 2012.
- Western Regional Climate Center (WRCC): https://wrcc.dri.edu/, last access: 18 September 2020, 2005.
 - You, C. F., Lee, T., and Li, Y. H.: The partition of Be between soil and water. Chemical Geology, 77(2), 105-118, https://doi.org/10.1016/0009-2541(89)90136-8, 1989.

Figures

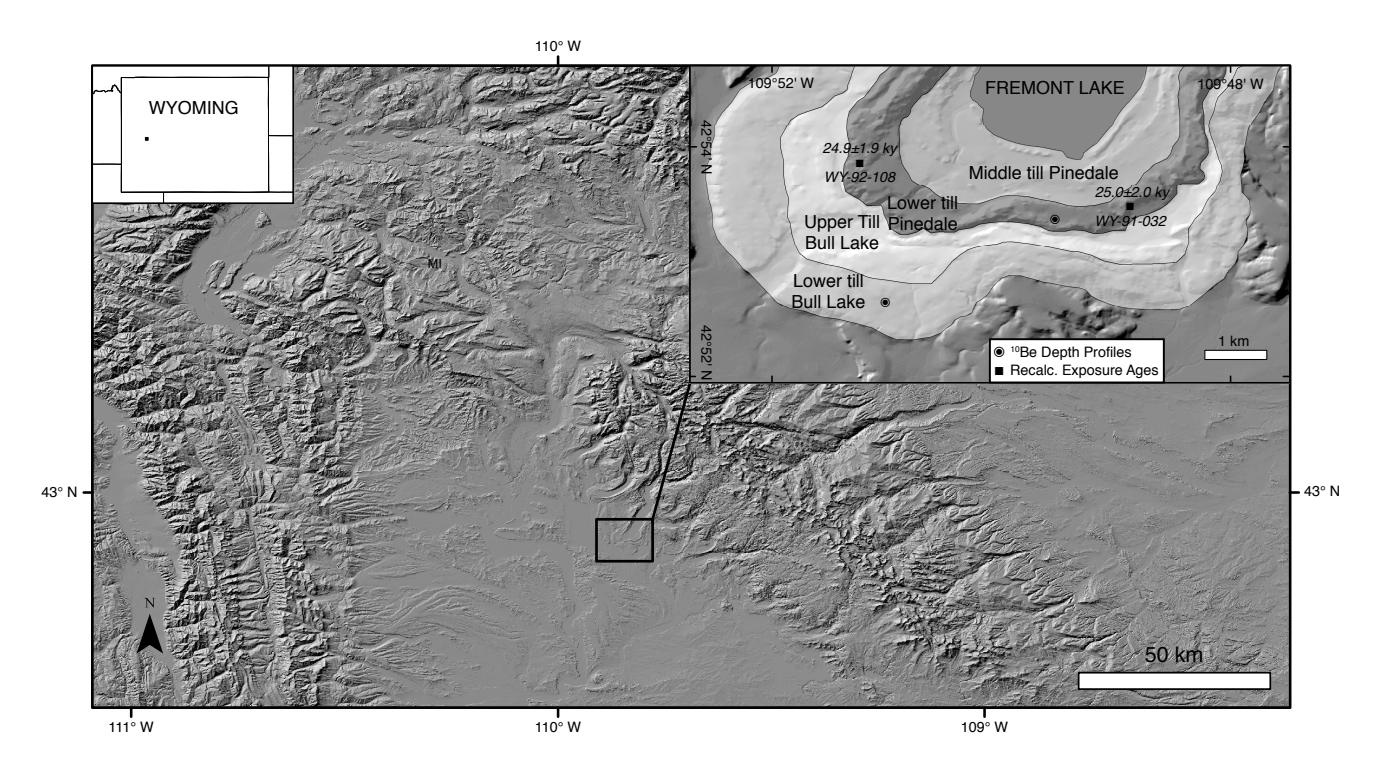


Fig. 1) Hillshade map of the Wind River range, derived from a 10 m digital elevation model (DEM); regional map encompasses the entirety of the meteoric ¹⁰Be flux map grid cell of Heikkila and von Blanckenburg (2015). Inset (upper left) shows location of regional map within Wyoming. Inset (upper right) shows locations of depth profiles analyzed for cosmogenic nuclide concentrations from the terminal Pinedale and Bull Lake moraines in the Fremont Lake area (after Richmond, 1973 and Schaller et al., 2009a). Also shown are the locations of boulder surface exposure dates for the Pinedale moraine (WY-92-108 and WY-91-032 of Gosse et al., 1995) that were recalculated using revised parameters (Table S1) to establish an updated independent age constraint for this moraine.

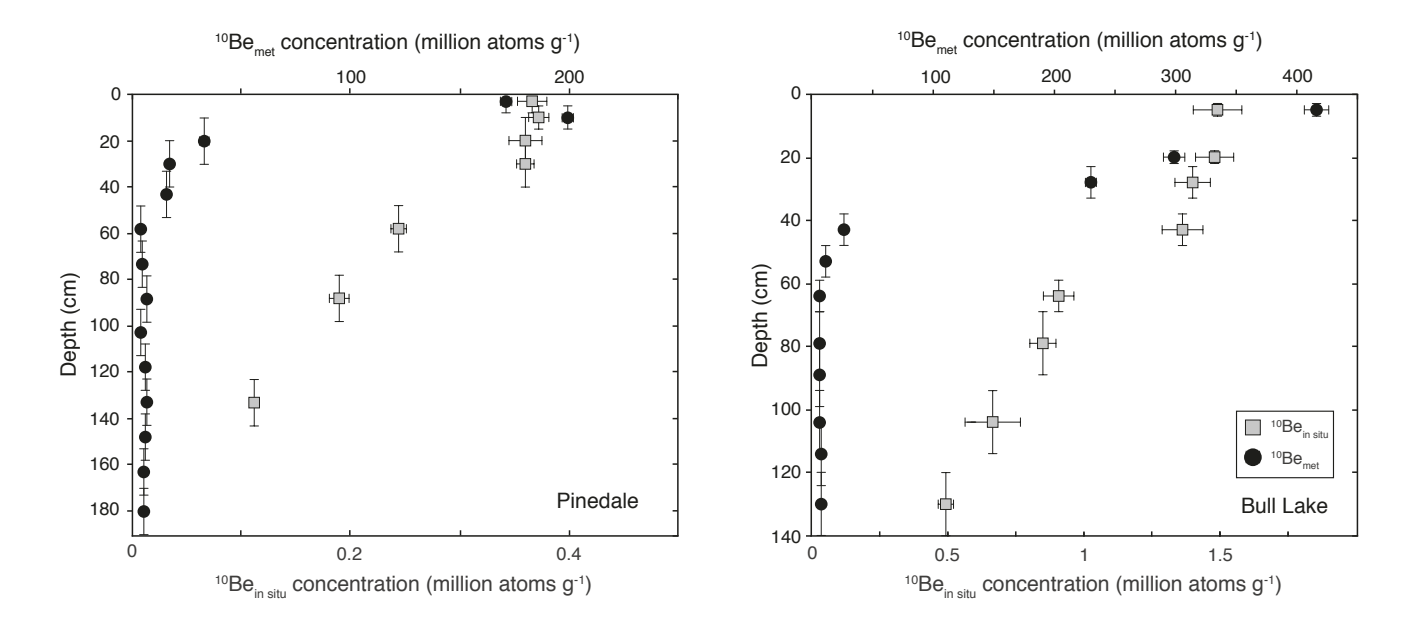


Fig. 2) (Left) Depth profile for the Pinedale moraine; 10 Be_{met} concentrations were measured from the <2 mm grain-size fraction of 14 samples from the same depth profile as analyzed for 10 Be_{in situ} in Schaller et al. (2009a). (Right) Depth profile for the Bull Lake moraine; 10 Be_{met} concentrations were also measured from the <2 mm grain-size fraction of 11 samples from the same depth profile as analyzed for 10 Be_{in situ} in Schaller et al. (2009a). The 10 Be_{met} concentration at 94 cm was not measured.

Table 1. Recalculated Chi-Square Solutions for Different Denudation Rate Simulations of Schaller et al. (2009a)^a

Type of Denudation	Model	Age (ky; fixed parameter)	Average Denudation (mm ky ⁻¹)	Inherited ¹⁰ Be concentration (10 ⁵ at g ⁻¹)	Mixing Depth (cm)	Diffusivity k $(10^{-3} \text{ m}^2 \text{ y}^{-1})$	Maximum Height (m)	Slope Angle (degrees)	
		Pinedale mo	raine (2262 m a	usl, 42° 53′ 26″ N,	109° 49′ 34	4" W)			
Constant	2	25	15	0.2	0				
Transient	4	25	29-35	0.2	0	20	30	25,30	
Bull Lake moraine (2285 m asl, 42° 52′ 39″ N, 109° 51′ 00″ W)									
Constant	6	140	7.5	1.4	0				
Transient	8	140	6-21	1.2-1.8	0	0.3-10	35,40,50,60	5,10,15, 20,25,30	

^aFor a full explanation of range allowed and resolution of each parameter, see Table 3 of Schaller et al. (2009a)

Table 2. ¹⁰Be Concentrations and GSD^a in Depth Profiles from Pinedale and Bull Lake Moraines

Sample ^b	Depth (cm)	Sand (wt %)	Silt (wt%)	Clay (wt %)	In situ ¹⁰ Be concentration ^c (10 ⁵ atoms g ⁻¹)	Meteoric 10Be sample weight (g)	⁹ Be carrier weight (mg)	Meteoric ¹⁰ Be concentration ^c (10 ⁶ atoms g ⁻¹)	Meteoric ¹⁰ Be inventory ^d (10 ⁶ atoms cm ⁻²)
	(-)				m asl, 42° 53′ 26			(1 1 8)	,
04-WRMP-		1 meaa	ic moran	10 (2202	ast, 72 55 26	11, 100 10	31 11)		
014	3 ± 2	75	18	6	3.67 ± 0.14	4.5747	0.2146	171.283 ± 5.142	1006 ± 30
04-WRMP-									
013	10 ± 5	68	22	10	3.73 ± 0.09	3.1697	0.2146	199.526 ± 5.986	2743 ± 84
04-WRMP- 012	20 ± 10	70	23	7	3.60 ± 0.15	6.4287	0.2146	33.007 ± 3.183	588 ± 64
04-WRMP-	20 ± 10	70	23	/	3.00 ± 0.13	0.4267	0.2140	33.007 ± 3.163	366 ± 04
011	30 ± 10	74	22	4	3.60 ± 0.08	6.1094	0.2148	16.819 ± 1.541	265 ± 31
04-WRMP-									
010	43 ± 10	76	19	5	-	5.1606	0.2144	15.357 ± 1.189	306 ± 31
04-WRMP-	5 0 + 10	02	1.5	2	2.44 + 0.07	<i>5 (17</i> 0	0.2146	2.066 + 0.226	11 + 10
009 04-WRMP-	58 ± 10	82	15	3	2.44 ± 0.07	5.6470	0.2146	3.966 ± 0.336	11 ± 10
008	73 ± 10	85	12	3	_	5.4438	0.2142	4.673 ± 0.382	33 ± 11
04-WRMP-									
007	88 ± 10	81	16	3	1.89 ± 0.09	5.6027	0.2140	6.699 ± 0.563	94 ± 17
04-WRMP-	100 : 10	0.0		2		6.006	0.0100	2.560 . 0.222	0 . 10
006 04-WRMP-	103 ± 10	82	15	3	=	6.0067	0.2103	3.569 ± 0.322	0 ± 10
005	118 ± 10	71	23	6	_	3.0500	0.2127	6.207 ± 0.284	79 ± 9
04-WRMP-	110 = 10	, 1	23	O		3.0300	0.2127	0.207 = 0.201	7,7 = 7
004	133 ± 10	71	24	5	1.11 ± 0.03	3.1070	0.2134	6.489 ± 0.302	88 ± 9
04-WRMP-									
003	148 ± 10	74	21	6	-	2.9340	0.2128	5.656 ± 0.249	63 ± 7
04-WRMP- 002	163 ± 10	72	22	6		2.8869	0.2107	5.531 ± 0.240	59 ± 7
04-WRMP-	103 ± 10	12	22	O	-	2.0009	0.2107	3.331 ± 0.240	39 ± 7
001	180 ± 10	72	23	6	-	3.0824	0.2135	5.098 ± 0.236	52 ± 8
								ſ	5387 ± 122
		Bull La	ake mora	ine (228.	5 m asl, 42° 52′ 39	0" N. 109° 51	' 00" W)	·	
AT-FL-4L	5 ± 2	69	22	9	14.9 ± 0.9	1.0174	0.4125	415.475 ± 12.464	4092 ± 125
		51		20	14.8 ± 0.7	1.0793	0.2139		
AT-FL-4K	20 ± 5							298.813 ± 8.965	8774 ± 269
AT-FL-4J	28 ± 5	52	34	14	14.0 ± 0.6	1.0824	0.2140	230.442 ± 6.913	3585 ± 111
AT-FL-4I	43 ± 5	47	23	30	$12.3^{\text{m}} \pm 0.7$	1.0593	0.1963	26.590 ± 0.798	608 ± 24
AT-FL-4H	53 ± 5	50	28	22	-	1.0176	0.2141	11.433 ± 0.343	102 ± 7
AT-FL-4G	64 ± 5	54	26	20	9.08 ± 0.56	1.0109	0.2144	7.083 ± 0.382	17 ± 8
AT-FL-4F	79 ± 10	60	24	16	8.50 ± 0.48	1.01	0.2141	6.639 ± 0.236	10 ± 7
AT-FL-4E	89 ± 10	62	24	14	<u>-</u>	1.0722	0.2142	6.318 ± 0.246	0 ± 5
AT-FL-4D	94 ± 10	75	17	9	_		0,2112	6.723 ^e	0 ± 5 4e
A1-FL-4D	74 ± 10	13	1 /	フ	-	-	-	0.723	+

AT-FL-4C	104 ± 10	64	26	10	$5.98^{\text{m}}\pm1.00$	1.0164	0.2144	7.129 ± 0.428	16 ± 9
AT-FL-4B	114 ± 10	60	25	15	-	1.0283	0.2142	8.021 ± 0.241	34 ± 5
AT-FL-4A	130 ± 10	60	25	15	4.93 ± 0.28	1.0294	0.2143	8.449 ± 0.253	68 ± 8
								ſ	17310 ± 318

^aGrain size distributions and *in situ* ¹⁰Be concentrations from *Schaller et al.* (2009a)

Table 3. ¹⁰Be_{met} flux estimates, raw and normalized for Holocene paleointensity variations

Method	$F(^{10}Be_{met})$ uncorrected (x 10^6 atoms cm ⁻² y ⁻¹)	Valid over time scale (ky)	¹⁰ Be _{met} production ratio relative to Modern	¹⁰ Be _{met} production ratio relative to Holocene	F(¹⁰ Be _{met}) corrected to represent Holocene (x 10 ⁶ atoms cm ⁻² y ⁻¹)
Pinedale (This Study)	1.04 (±0.14)	6	0.88^{a}	0.71ª	1.46 (±0.20)
Bull Lake (This Study)	1.04 (±0.39)	24	0.99^{a}	0.80^{a}	1.30 (±0.48)
Graly et al. (2011)	$0.55~(\pm~0.05)$	0.005	0.82^{b}	0.67°	0.83 (±0.08)
Heikkilä and von Blanckenburg (2015)	-	10	1.23°	-	1.38 (+0.99) ^d

 $^{^{}a}$ using measured 10 Be $_{met}$ seafloor accumulation record of Christl et al. (2010) from

^bSee Schaller et al. (2009a) for the grain size fraction analyzed for each sample

^cCorrected for blank, reported error includes analytical uncertainties (1σ)

^dCorrected for inheritance

^eAverage of ¹⁰Be_{met} concentations from directly above and below this depth

^aAverage of multiple aliquots analyzed in Schaller et al. (2009a)

⁶ ky and 24 ky to present for the Pinedale and Bull Lake moraines, respectively

^b using the paleomagnetic scaling method of Masarik and Beer (2009)

^c using the paleomagnetic reconstruction method of Steinhilber et al. (2012)

^d uncertainty represents the difference between the 'industrial' and the 'pre-industrial' modeled flux of Heikkilä and von Blanckenburg (2015)